Structure of Polyelectrolyte Stars and Convex Polyelectrolyte Brushes

Sanjay Misra,*,† Wayne L. Mattice,† and Donald H. Napper‡

Institute of Polymer Science, The University of Akron, Akron, Ohio 44325-3909, and School of Chemistry, The University of Sydney, Sydney, NSW 2006, Australia

Received May 31, 1994; Revised Manuscript Received August 23, 1994®

ABSTRACT: The structure of polyelectrolyte stars and spherical brushes is discussed using a local force balance argument that balances the osmotic pressure and the tension in the chains locally for a given radial position. In general, there are four distinct regions where the segment density profile $\Phi(r)$ is dominated by one of the interactions: (i) in the outer region, electrostatic interactions dominate, (ii) in the intermediate region, binary interactions dominate, (iii) in the inner region ternary interactions dominate, and finally (iv) at the center of the star (of the order of a few segment lengths), the density is unity. For poor solvents we predict a collapse induced by the attractive binary interactions that leads to a two-phase star or brush. The inner dense layer is stabilized by ternary interactions whereas the outer dilute layer is dominated by electrostatic repulsions—the segment density changes discontinuously from one to the other (and the intermediate density region disappears). The magnitude of the collapse transition is found to increase with the chain length for stars and spherical brushes, unlike planar brushes. The star is expected to collapse continuously with the reduction in the solvent quality—unlike a first-order transition for planar brushes. Planar polyelectrolyte brushes can also display two-phase regions; however, the full SCF approach is warranged in this case. Collapse induced by n-clusters in uncharged polymers is also shown to lead to two-phase brushes.

1. Introduction

Tethered polymer chains play an important role in areas as wide-ranging as colloid stability, compatibilization, rheology control, and membrane modification. The case of layers formed by the dense tethering of long chain polymers onto a surface, the so-called brushes, has received much attention in recent years, in theoretical as well as experimental terms, due to their technological importance.[1]

The case of planar brushes in good solvents was first studied by Alexander[2] and de Gennes[3] under the assumption that the free ends of the tethered chains all lay in the same plane (and hence that the segment density in the brush was constant). This model, while approximate, faithfully reproduces many of the general scaling features of brushes. The assumption that the chain ends lie in the same plane was relaxed by Milner, Witten, and Cates (MWC)[4] and independently by Zhulina and co-workers[5] in their self-consistent field (SCF) theories. Milner et al. showed that the polymer segment potential in the brush varies parabolically with the distance from the surface. Using an appropriate equation of state for the segment potential, one can then deduce the segment density profile in the brush; the profile itself is almost parabolic under moderate concentration conditions. Paralleling the developments in the theory for brushes in good solvents, the structure of brushes in poor solvents was addressed in the Alexander–de Gennes approximation by Halperin,[6] Halperin and Zhulina,[7] Zhulina et al.,[8] Lai and Halperin,[9] and Lai.[10] The self-consistent field picture was generalized to poor solvents by Shim and Cates[11] and also by Zhulina et al.[8] Uncharged mesogels (chains tethered by both ends between two surfaces leading to both loops and bridges) have also been investigated by Halperin and Zhulina[12] in the Alexander–de Gennes approximations, by Johner and Joanny,[13] Zhulina and Pakula,[14] Milner and Witten,[15] and Halperin and Zhulina[16] using the SCF theory, and by Misra and Mattice using the Monte Carlo method.[17]

While the above developments focused on uncharged polymers, considerable interest exists in the use of water-soluble polymers which are most often polyelectrolytes. The Alexander–de Gennes model was generalized to polyelectrolyte brushes under all solvency conditions by Pincus,[18] Zhulina and co-workers,[19,20] and Pincus and Ross.[21] These works addressed the collapse transition of polyelectrolyte brushes in a poor solvent. They did not, however, discuss the structure within the brush, i.e., the segment density distribution, for either planar or curved surfaces (although some general picture of the phase transitions of curved brushes emerged). The step function model was also used to discuss the self-association and surface association of diblock copolymers (one block being a polyelectrolyte) by Argillier and Tirrell,[22] Wittmer and Joanny,[23] and Dan and Tirrell.[24] The extension of the SCF method to polyelectrolytes by Miklavic and Marcelja,[25] by Misra et al.,[26–28] and by Zhulina et al.[29] addressed the structure of brushes (i.e., the segment density distribution) in good solvents but they did not consider the poor solvent case. (Charged mesogels, closely related to the brushes, have also been treated recently using both the Alexander–de Gennes approximation[20,30] and the SCF picture.[20])

In what follows, we show that the nonuniformity of the segment density in the polyelectrolyte brush can lead to interesting changes in the structure with poor solvent conditions. We begin with a polyelectrolyte brush in good solvent conditions where in general (for planar or convex brushes) the segment density decreases away from the surface. As the solvent quality is lowered, the binary interactions become attractive instead of repulsive. In the outer part of the brush, where the segment density is lower, the electrostatic repulsions still dominate. However, in the inner region of the brush where the segment density is larger, the binary attractions can overcome the electrostatic repulsion. The inner region can collapse (its density is determined by a balance between the ternary and elastic forces) while an outer dilute layer survives (stabilized by the repulsive electrostatics). This leads to a brush with an inner dense (or collapsed) layer and an outer dilute (or stretched) layer. (We point out later that

* email: misra@polymer.uakron.edu.
† The University of Akron.
‡ The University of Sydney.
® Abstract published in *Advance ACS Abstracts*, October 15, 1994.

0024-9297/94/2227-7090$04.50/0

this collapsed structure is analogous to that induced by n-clusters[31,32] in uncharged brushes. In this case, according to de Gennes,[31] the binary attractions can be repulsive and some higher order interactions attractive.)

In this work we look at the collapse of polyelectrolyte brushes tethered to convex surfaces (outer surface of a cylinder or a sphere). This situation is also directly relevant to the study of polyelectrolyte stars as well as graft copolymers with bottle brush-like architecture as well (particle or cylinder radius tending to zero). Indeed much of the literature on star or branched polymers deals with uncharged polymers using scaling or Flory type pictures,[33-38] renormalization group theory,[39] Monte Carlo or lattice models,[40-42] or molecular dynamics methods.[43] Much of the interest in their properties arises from their potential application as rheology modifiers. In this context it would be useful to look at polyelectrolyte stars as well, since water-soluble polymers are acquiring increasing industrial importance.

We assume, in the spirit of the Alexander–de Gennes model, that the chain ends all lie at the same distance from the cylinder axis or the center of the sphere. A simple force balance argument which balances the local tension in the chains to the local osmotic pressure yields non-uniform density profiles for convex brushes. Under poor solvent conditions these brushes show a dense inner layer next to the grafting surface and a dilute outer layer, the density change being continuous from one to the other.

The approximation of all chain ends lying in the same shell can be relaxed by following the SCF approach of Ball et al.[44] Indeed for convex brushes this SCF work shows that an exclusion zone exists next to the surface from which chain ends are excluded, and the approximation of all chain ends lying in the same shell is not as severe as for planar brushes.[44] In any case we expect that the full SCF picture will also predict a discontinuous segment density profile for convex polyelectrolyte brushes in a poor solvents, arising from the appearance of two stable branches to the solution of the SCF potential equation.

While the main body of the paper is concerned with the Alexander–de Gennes type picture for the stars and spherical brush, we also address the cylindrical and planar polyelectrolyte brushes in the appendices. It is shown that the density change in a planar brush can also be discontinuous but one does need to resort to the self-consistent field method of Milner et al. in that case.

The rest of the paper is organized as follows. In the next section we develop the mean field model for spherical brushes. We study the consequences of this model for stars and spherical brushes in good solvents and compare these with the existing works in section 3. In section 4 we show some typical segment density profiles for polyelectrolytes in poor solvents and outline the Maxwell construction needed to determine the point of discontinuity. We also make some predictions relating to the phase transitions in spherical polyelectrolyte brushes based on the present model. In section 5 we look at the structure of spherical brushes collapsed by n-clusters. Conclusions are presented in section 6. Appendix 1 summarizes the results obtained for cylindrical brushes or bottle brush polymers using the present model. In Appendix 2 we look at planar polyelectrolyte brushes in poor solvents using the SCF approach of MWC, along the lines suggested by the work of Wagner et al.[32]

2. Model for Stars and Spherical Brushes

The local structure of the brush is governed by a local balance between the stretching of chains, the osmotic pressure (arising from polymer segments and the counterions), the local electric field), and any external forces. In the Alexander–de Gennes picture all chains contribute equally to the local stretching and osmotic pressure. For a planar brush the Alexander–de Gennes picture implies that the segment density and the stretch are uniform in the brush. (In the SCF picture of MWC the local stretching of chains is different since the chain ends are distributed all over the brush. The chains thus contribute to a different extent to the local force balance.)

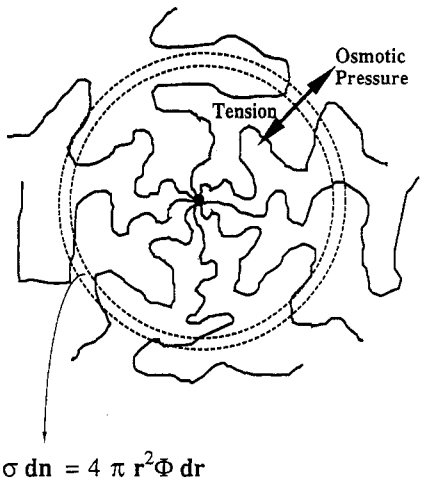

Figure 1. Schematic representation of a star (or spherical brush) showing the local balance between the tension in the chains and the osmotic pressure.

Even if one uses an Alexander–de Gennes type model for a spherical brush (all free chain ends lie at the same outer shell), one cannot assume a constant density. This is because a constant density implies that the osmotic pressure is constant as one goes outward. However, due to the increasing amount of available volume, the stretching rate decreases (to keep the density constant), implying a local imbalance of forces. Similarly, a constant stretching rate would imply a continuous drop in the osmotic pressure as one went outward in the brush, and hence the force balance is not satisfied. One thus needs to resort to a local balance of forces.

2.1. Force Balance for Stars and Spherical Brushes. Consider a spherical particle of radius r_0 with σ_0 chains grafted per unit area of the surface. If the segment density is given as $\Phi(r)$, then we have (Figure 1)

$$4\pi r^2\Phi\, dr = 4\pi r_0^2\sigma_0\, dn \rightarrow \frac{dr}{dn} = \frac{r_0^2\sigma_0}{r^2\Phi} \qquad (1)$$

where each chain contributes dn segments to a shell of thickness dr at distance r from the center of the sphere. In the case of a star polymer with σ identical arms, one can replace the product $(r_0^2\sigma_0)$ with $(\sigma/4\pi)$. Depending upon whether one is discussing star polymers or brushes, it is useful to use either σ or both σ_0 and r_0. Note that (dr/dn) is the local tension in the chain that must be balanced by the osmotic pressure. The tension transmitted at any shell per unit area is $(r_0^2\sigma_0/r^2)\, dr/dn$ and must be balanced by the local osmotic pressure Π (Figure 1)

$$\Pi = \left(\frac{\sigma_0 r_0^2}{r^2}\right)\left(\frac{\sigma_0 r_0^2}{r^2\Phi}\right) \qquad (2)$$

Rearranging and substituting $\bar{r} = (r/r_0\sigma_0^{1/2})$, one can rewrite

eq 2 as

$$\Phi\Pi = 1/\bar{r}^4 \tag{3}$$

The solutions to this equation provide the reduced segment density profiles from which one can extract any particular profile for given values σ_0 and r_0. The osmotic pressure Π is given as

$$\Pi = \Phi\frac{\partial F}{\partial \Phi} - F \tag{4}$$

where F is local free energy density. We assume local electroneutrality in which case the free energy density due to the electric field disappears and the local volume fraction of the counterions is the same as that of the dissociated segments. We can write the Flory–Huggins type of expression

$$F_{\text{Flory}}(\Phi) = (1-\Phi)\ln(1-\Phi) + \chi\Phi(1-\Phi) + f\Phi\ln f\Phi \tag{5a}$$

where the first two terms are the familiar solvent translational entropy and the enthalpy of mixing. χ is the Flory–Huggins parameter, and f is the fraction of dissociated polymer segments. The last term represents the translational entropy of the counterions. The osmotic pressure is therefore given as

$$\Pi_{\text{Flory}} = -\ln(1-\Phi) - \chi\Phi^2 - (1-f)\Phi \tag{5b}$$

Alternatively, one can use the truncated virial expansion for the free energy density, which is useful for obtaining analytical solutions of eq 4, although the density saturation effects are not as faithfully represented as the Flory–Huggins expression. One can write[20,21,30]

$$F_{\text{virial}} = \frac{1}{2}\nu\Phi^2 + \frac{1}{6}\Phi^3 + f\Phi\ln f\Phi \tag{6a}$$

where ν is the excluded volume parameter and we assume that the ternary interaction parameter is unity (as implied by the expansion of the Flory–Huggins expression). In this case the osmotic pressure becomes

$$\Pi_{\text{virial}} = \frac{1}{2}\nu\Phi^2 + \frac{1}{3}\Phi^3 + f\Phi \tag{6b}$$

We would like to point out that the electrostatic contribution to the free energy and the osmotic pressure as expressed above, in eqs 5 and 6, relies on the local electroneutrality condition. This requires that most of the counterions are confined to the star molecules—a condition that is fulfilled when the largest Debye screening length in the star is much smaller than the dimensions of the star. As shown in the next section, the size of a polyelectrolyte star $R_P \sim f^{1/2}N$. The segment density in the outer region of a polyelectrolyte star $\Phi \sim \sigma f^{-1/2}r^{-2}$. The square of the local Debye screening length is given as $\kappa^{-2} = 1/(4\pi l_b f\Phi)$, where l_b, the Bjerrum length, is given as e^2/kT (e is the protonic charge, k is the Boltzmann constant, and T is the temperature). The maximum value of κ^{-1} occurs at the periphery of the star where $\Phi \sim \sigma f^{-1/2}/R_P^2$. Requiring that $R_P/\kappa^{-1} \gg 1$ leads to the following condition under which local electroneutrality may be assumed—$(fl_b\sigma)^{1/2} \gg 1$. Thus eqs 5 and 6 have greater validity for stars with greater charge and larger number of arms, such that the previous inequality is satisfied.

3. Stars and Spherical Brushes in Good Solvents

We now look at the consequences of the above equations for star polymers and spherical brushes in good solvents.

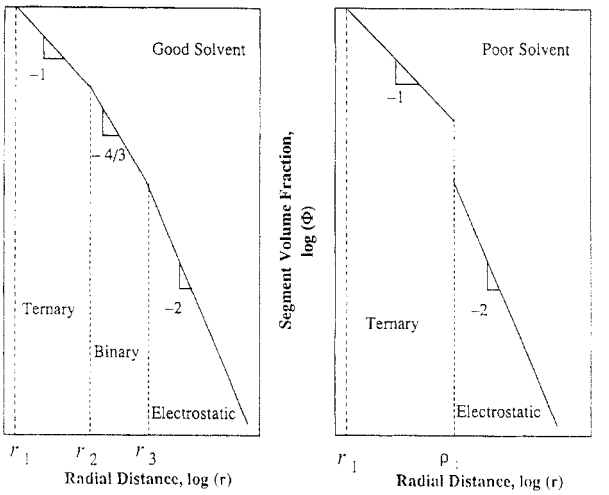

Figure 2. General features of the density profiles of polyelectrolyte stars and spherical brushes in good and poor solvents. The scaling of density with radial distance is shown as are the crossover distances where the scaling changes from one form to another.

We use eq 6b for the osmotic pressure, with the caveat that for star polymers close to the center the density is very high (approaching the melt density near the center) and therefore eq 6b is probably not very appropriate near the center of the star. A summary of the results presented below is provided in Figure 2.

3.1. Segment Density Profiles. In the outermost part of the star the density is very low and electrostatic interactions will dominate. Accordingly we have ($\Pi \sim f\Phi$)

$$f\Phi^2 = \frac{\sigma^2}{16\pi^2 r^4} \rightarrow \Phi \sim f^{-1/2}\sigma^1 r^{-2}, \quad \text{outermost region } (r_3 < r) \tag{7}$$

This implies that the stretch rate is a constant from eq 1! As we noted in section 2, one generally expects both the stretching and the volume fraction to vary with the radial position in order to balance the forces locally. Only under the electrostatics-dominated case do we satisfy the local force balance by constant stretching. The chains, in this regime, are greatly stiffened by electrostatic repulsions. As one moves further into the star and as the density rises one goes from an electrostatic to a binary interactions dominated regime. The crossover occurs when the binary and electrostatic terms are comparable, i.e., when $\Phi \approx (2f/\nu)$. Substituting this in eq 7, we obtain that the crossover between binary- and electrostatic-dominated regions occurs at $r_3 \sim (\sigma\nu)^{1/2}f^{-3/4}$. For $r_2 < r < r_3$ the segment density profile is dominated by binary repulsions and $\Pi \sim \nu\Phi^2$, leading to the following density profile:

$$\frac{1}{2}\nu\Phi^3 = \frac{\sigma^2}{16\pi^2 r^4} \rightarrow \Phi \sim \nu^{-1/3}\sigma^{2/3}r^{-4/3}, \quad \text{intermediate region } (r_2 < r < r_3) \tag{8}$$

This density profile is in agreement with the corresponding results of Daoud and Cotton.[33] Note that the stretching rate is proportional to $r^{-2/3}$ (unlike r^0 in the electrostatic regime). At smaller radii, $r < r_2$, where the ternary repulsions are stronger than the binary repulsions we have $\Pi \sim \Phi^3$ and we obtain

$$\frac{1}{3}\Phi^4 = \frac{\sigma^2}{16\pi^2 r^4} \rightarrow \Phi \sim \sigma^{1/2}r^{-1}, \quad \text{inner region } (r_1 < r < r_2) \tag{9}$$

Again this is in agreement with the model of Daoud and Cotton[33] for uncharged stars. The crossover between intermediate and inner regions occurs when the binary and ternary terms are comparable, i.e., when $\Phi \approx (3\nu/2)$. Substituting this result in eq 9, we obtain that the crossover radius $r_2 \sim \sigma^{1/2}\nu^{-1}$, also in agreement with the Daoud and Cotton result. Finally, very near the center, $r < r_1$, one has a melt density ($\Phi \approx 1$). The terms on the right-hand side of eq 2 are of order unity and we get $r_1 \sim \sigma^{1/2}$.

3.2. Dimensions of Star Polyelectrolytes. For given solvency conditions the star can be in states dominated primarily by ternary, binary, or electrostatic interactions depending upon the chain length of the arms. Knowing both the crossover distances where the scaling of density profile changes and the respective scaling of the density profiles, one can determine the range of chain lengths that puts the star in one regime or another. We obtain the following results (which can be rearranged to look at the effects of changing charge fraction, f, or excluded volume interactions, ν)

$$(\sigma\nu)^{1/2}f^{-5/4} \ll N, \quad \text{polyelectrolyte regime} \tag{10a}$$

$$\sigma^{1/2}\nu^{-2} \ll N \ll (\sigma\nu)^{1/2}f^{-5/4}, \quad \text{binary repulsion regime} \tag{10b}$$

$$\sigma^{1/2} \ll N \ll \sigma^{1/2}\nu^{-2}, \quad \text{ternary repulsion regime} \tag{10c}$$

The radius of the star polymer can be obtained by integrating the density profile

$$\sigma N = \int_0^R dr\, \Phi(r)(4\pi r^2) \tag{11}$$

For a star molecule that is dominated by the electrostatic repulsions (eq 10a), corresponding to very long chains or when $f > 0$ and $\nu \approx 0$, we obtain using eq 11

$$R_P \sim \sigma^0 f^{1/2} N^1, \quad \text{polyelectrolyte regime} \tag{12}$$

The subscript P refers to polyelectrolytes. We note that the radius of the star is independent of the number of arms in the star! This is surprising until one notes that the chains are very strongly stretched since $R_P \sim N$ (as against binary repulsions dominated star where $R_B \sim N^{3/5}$; see below). Thus lateral repulsions that show up in the arm number dependence are alleviated and the radius of the star is independent of the arm number. This result was first obtained by Pincus[18] in his discussion of polyelectrolyte brushes grafted to colloids (porcupines) and by Zhulina[20] for charged spherical mesogels; both of these works used a global energy balance argument where the density in the spherical shell was taken to be constant.

For charged polymers, with relatively shorter arms, the following results are in complete agreement with the previous works on uncharged stars. Under binary repulsion regime (eq 10b), corresponding to intermediate chain lengths or when $f = 0$ and $\nu > 0$, the following well-known result is derived (see for example refs 1, 33, and 38)

$$R_B \sim \sigma^{1/5}\nu^{1/5}N^{3/5}, \quad \text{binary regime} \tag{13}$$

The subscript B refers to binary repulsions. Note that the arm number dependence is not very strong and so it is easily eliminated once the chains are swollen even further by electrostatic repulsions.

For even shorter stars chains (eq 10c), or when $\nu \approx f \approx 0$, we have a ternary repulsions dominated star[1,33,38]

$$R_T \sim \sigma^{1/4}N^{1/2}, \quad \text{ternary regime} \tag{14}$$

The subscript T refers to ternary repulsions.

Another noteworthy quantity is the ratio R_P/R_B, which is a measure of the magnitude by which the dimensions of a polyelectrolyte star would change when it contracts by a reduction in the charge fraction on the backbone (i.e., when it goes from the polyelectrolyte-dominated regime to the excluded volume regime).

$$R_P/R_B \sim \sigma^{-1/5}N^{2/5} \quad (P \rightarrow B) \tag{15}$$

The transition becomes more pronounced as the grafting density or the number of arms is reduced, i.e., for more dilute brushes and stars. Interestingly, the transition now depends upon the chain length (unlike planar brushes where the ratio is independent of the chain length, as shown by Ross and Pincus[21]) and becomes stronger as the chain length increases ($N \gg 1$). Indeed the collapse would be more pronounced for spherical brushes rather than for planar brushes, in agreement with the work of Zhulina on charged mesogels.[20] The relative volume change upon collapse for spherical brushes and stars is obtained by cubing the ratios in eq 15 (whereas for planar brushes it is proportional to the first power of the ratios) and is even more dramatic.

For very poor solvents (or very short chains) the brush or star can be made to collapse into a dense phase with the volume fraction $\Phi \sim 1$. For totally collapsed stars (or spherical brushes) the radius of the dense structure $R_D \sim \sigma^{1/3}N^{1/3}$.

Thus the ratios

$$R_P/R_D \sim \sigma^{-1/3}N^{2/3} \quad (P \rightarrow D) \tag{16a}$$

and

$$R_B/R_D \sim \sigma^{-2/15}N^{4/15} \quad (B \rightarrow D) \tag{16b}$$

indicate that even the transition from a star swollen by repulsive binary interaction to total collapse is made quite strong for long chains ($N \gg 1$). Indeed for long polyelectrolyte stars the collapse is even more pronounced. Note again the N dependence in eq 16 which is absent for planar brushes.

4. Segment Density Profiles and Collapse in Poor Solvents

4.1. Segment Density Distribution. We now come to the segment density profiles obtained using the above model in poor solvents. In this section we use the Flory–Huggins theory for the most part since it faithfully represents the density saturation effect that creates a melt density at the center of the star and for brushes grafted under high density.

We show in Figure 3 typical density profiles in dimensionless coordinates where the osmotic pressure was calculated using eq 5b. The charge fraction is fixed at 0.1 and we vary χ between 0.8 and 0.94. Below a critical value of $\chi = \chi_c$ (0.91 in this case), the density profiles are single valued. Above $\chi = \chi_c$ the profiles have the following features (Figure 4): for $r < \rho_1$ the profile is single valued and is in what we shall call the dense region, for $\rho_1 < r < \rho_2$ the profile is in general three valued (in this region a discontinuous density change takes place from the upper

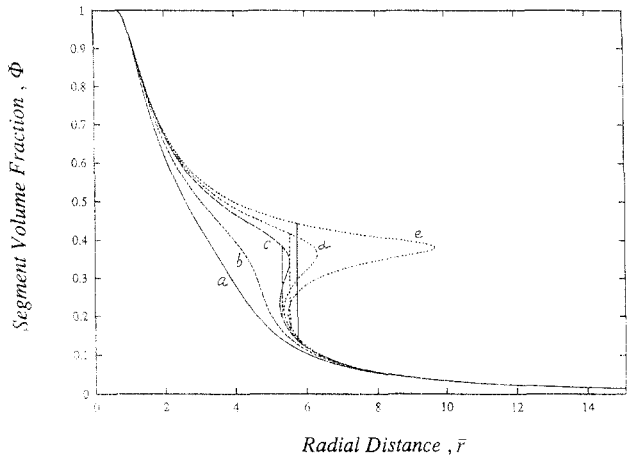

Figure 3. Reduced segment density profiles for polyelectrolyte stars and spherical brushes. The charge fraction $f = 0.1$. Equation 5b was used for calculating the osmotic pressure. The Flory–Huggins parameters χ are (a) 0.8, (b) 0.88, (c) 0.91, (d) 0.92, and (e) 0.94. The vertical lines, drawn using a Maxwell construction, show the discontinuous drop from the higher to the lower value.

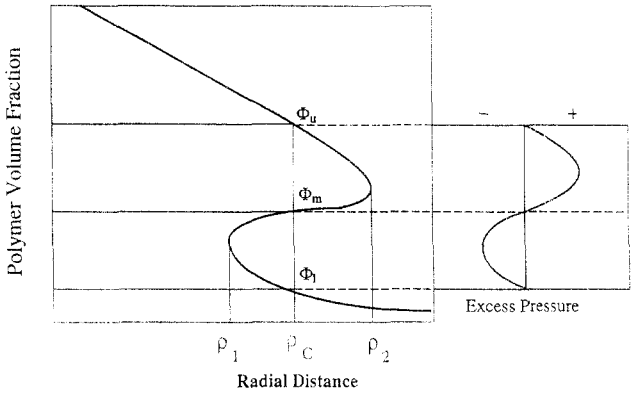

Figure 4. Schematic representation of a typical segment density profile in poor solvents, marking the points of interest.

to the lower value; the middle value is physically meaningless), and finally for $r > \rho_2$ the density profile is single valued again and is in the so-called dilute region. The solid vertical lines correspond to the Maxwell construction which determines the location where the discontinuous density change occurs.

The binary attractions being attractive overcome the electrostatic repulsions at a location in the star where the segment density is sufficiently high, leading to a collapsed inner region dominated by ternary repulsions. In the outer dilute layer electrostatic repulsions still dominate. Thus in a single polyelectrolyte brush we have two coexisting phases. The point of discontinuity can be evaluated by using a Maxwell construction that is in the same vein as the method employed in the case of cubic equations of state in vapor–liquid equilibrium (vapor corresponding to the dilute outer phase and liquid corresponding to the inner dense layer). In Figure 5 we show typical density profiles for a constant value of $\chi = 0.8$ and various values of charge fractions.

4.2. Maxwell Construction. We have the following equation of state (EOS) in the star or spherical brush that relates the excess pressure p to the local specific volume $V = 1/\Phi$. The excess pressure is the difference between the osmotic pressure and the tension in chains

$$p(V) = \Pi(\bar{V}) - V/\bar{r}^4 \qquad (17)$$

Note that the EOS depends upon the radial distance and hence each radial position has its own equation of

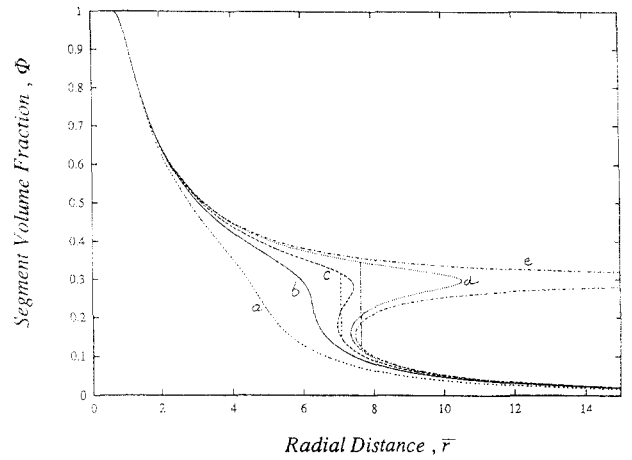

Figure 5. Reduced segment density profiles for polyelectrolyte stars and spherical brushes. The Flory–Huggins parameter $\chi = 0.8$. Equation 5b was used for calculating the osmotic pressure. The charge fractions are (a) 0.06, (b) 0.055, (c) 0.053, (d) 0.052, and (e) 0.051. The vertical lines show the discontinuous drop in the density.

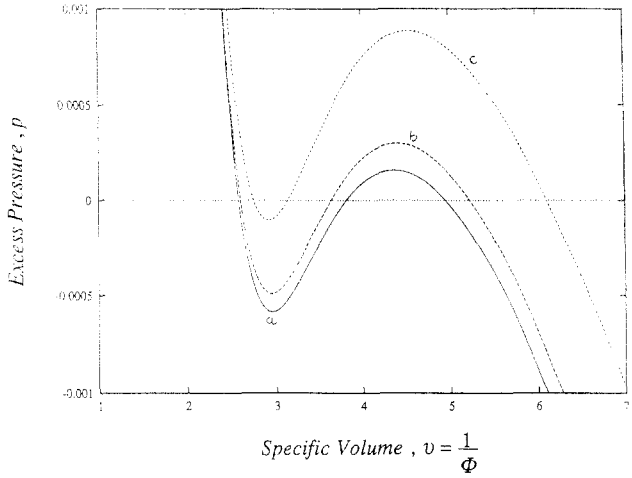

Figure 6. Typical p vs V diagrams at different radial locations for $\chi = 0.92$ and $f = 0.1$. Equation 5b was used for calculating the osmotic pressure. The radial positions are (a) 5.29, (b) 5.33, and (c) 5.48. At radius $\bar{r} = 5.33$, the areas above and below the curve are equal and a discontinuous density drop occurs at that location.

state. This is not surprising since each radial position represents a different local "grafting density". This corresponds to planar brushes with different grafting densities having different p–V diagrams. The density profiles correspond to the solution of eq 17 when $p = 0$. Let us construct a vertical line corresponding to a discontinuous density change at $r = \rho_C$ ($\rho_1 < \rho_C < \rho_2$) (Figure 4). As one moves from Φ_l to Φ_m the excess pressure starts at zero and becomes negative since stretching exceeds the osmotic pressure and goes again to zero at Φ_m. Between Φ_m and Φ_u the excess pressure is positive since the osmotic pressure exceeds the stretching. The net change in the chemical potential of the segments is just

$$\Delta\mu = \Delta(pV) - \int_{V_l}^{V_u} p\, dV = \int_{V_l=1/\Phi_l}^{V_u=1/\Phi_u} dV\, p(V) \qquad (18)$$

The radial position where the density changes discontinuously requires that $\Delta\mu = 0$. We show some typical p vs V profiles in Figure 6. Indeed for a spherical brush or star under a uniform radial compression corresponding to an external pressure p_E, one could recalculate the density profiles using eq 17 and in doing the Maxwell construction one would replace the integrand by $(p - p_E)$.

4.3. Collapse Transition. Upon changing the solvent quality from good to poor, the segment density profiles shift continuously, without any abrupt change (as does the location of the density discontinuity). Therefore, given a grafting density (number of arms) and chain length, we expect that the radius of the star or a brush (determined by the area under the Φ vs r^2 curves) will also change continuously with the change in solvent quality. While the magnitude of the collapse transition, on reducing either the solvent quality or the charge fraction, is much larger for these stars and spherical brushes, compared to planar brushes, and might appear first-order-like, the collapse, should be continuous instead of first order as predicted by Zhulina.[20] The disagreement as to the nature of the transition appears to be the result of a global energy balance employed by Zhulina where the density in the spherical mesogel is taken to be uniform unlike the local balance employed in the present work. Under poor solvency conditions, therefore, Zhulina's model predicts the coexistence of two brushes of different volume fractions and hence of two different thicknesses; the collapse is thus predicted as a first-order transition instead of a continuous change in the brush dimensions. On the other hand, the scaling results obtained for the dimensions of electrostatically swollen mesogels obtained by the uniform density model of Zhulina[20] are in complete agreement with the present work as shown in the previous section.

For a good solvent the polyelectrolyte arms are swollen and the density drops continuously. As the solvent quality decreases there appears an inflection point which is determined by the conditions

$$\partial\Phi\Pi/\partial\Phi = 0 \tag{19a}$$

and

$$\partial^2\Phi\Pi/\partial\Phi^2 = 0 \tag{19b}$$

The solution to eqs 19 determines the critical volume fraction at which the discontinuity first appears; substituting that value in eq 2 or 3 would give the critical value of the radial distance r_C. It can be shown that eqs 19 correspond to the condition that $\nu_C = -(128/27)^{1/2} f^{1/2} \approx -2.18f^{1/2}$; i.e., for a given value of f, the discontinuity first appears at ν_C.

As seen in the previous section, the structure of the brush in good solvents and the magnitude of the collapse transition depend upon the chain length. In the poor solvent domain ($\nu < \nu_C$) we essentially have only three regimes in the density profile: (i) the outer region dominated by electrostatics where the density profile $\Phi \sim r^{-2}$, (ii) an inner region dominated by ternary interactions where $\Phi \sim r^{-1}$, and (iii) a dense central region where $\Phi \approx 1$. The crossover from the ternary-dominated to the electrostatic-dominated regime, in poor solvents, can again be determined as follows.

While ρ_C marks the location where the dense and dilute phase are in equilibrium, the locations of ρ_1 and ρ_2 mark the boundaries of metastability. ρ_1 is the minimum distance where the density can change discontinuously. The location of ρ_1 is approximately determined by noting that here the density is lower and hence higher order terms can be neglected. Using only the binary interaction and electrostatic terms and setting $(\partial\Phi\Pi/\partial\Phi) = 0$, one can show that

$$\rho_1 \sim \sigma^{1/2}|\nu|^{1/2} f^{-3/4} \sim \sigma^{1/2}|1 - 2\chi|^{1/2} f^{-3/4} \tag{20}$$

Again, by changing the length of the arms (or by varying the solvent quality and the charge fraction), one can pass from an electrostatics-dominated regime to a ternary repulsions dominated regime. We can estimate approximately the crossover chain length N_{cross} at which one passes from a dense collapsed structure to a two-phase star or brush. If we assume that the density in the dense region falls inversely with r (ternary interactions dominate), i.e., $\Phi \sim r^{-1}$, then the radius of a star (or spherical brush) with shorter chains can be estimated as $R_T \sim \sigma^{1/4}N^{1/2}$ (eq 14). At the crossover value of the chain length $R_T \sim \rho_1$ and therefore we have

$$N_{cross} \sim \sigma^{1/2} f^{-3/2} |\nu| \tag{21}$$

Remember that $\sigma \sim \sigma_0 r_0^2$. Thus the crossover chain length increases linearly with the radius of the grafting particle for a constant surface coverage. Of course, for a given value of N and σ one could rearrange eq 21 to estimate $|\nu_{cross}|$. This indicates the extent to which the solvent quality would be lowered in order to obtain a totally collapsed star. As the equation indicates, a greater reduction in solvent quality would be necessary to completely collapse a star which has longer arms ($|\nu_{cross}| \sim N$) or one which has fewer arms ($|\nu_{cross}| \sim \sigma^{-1/2}$). The ratio of ternary-dominated and electrostatic-dominated regimes is obtained as

$$R_P/R_T \sim \sigma^{-1/4}N^{1/2} \quad (P \rightarrow T) \tag{22}$$

The collapse is stronger than collapse from a polyelectrolyte to a binary regime (eq 15), in good solvent, in terms of the grafting density or arm number as well as the chain length. The effect, correspondingly, on the stability and rheology of colloidal suspensions would be more dramatic as well. This is in contrast with planar brushes where the chain length does not qualitatively affect the structure of the brush itself.

The crossover values of N, σ, ν, or f have an additional significance in the poor solvent regime in terms of colloid stabilization. In the good solvency domain ($\nu > 0$) the passage from an electrostatic regime to a binary regime to a ternary regime changes the range and scaling of interaction between two sterically stabilized particles; the nature of the interaction itself remains repulsive. In the poor solvent region ($\nu < 0$), however, dense steric layers (ternary interactions regime) will be prone to *intermediate range* attractive forces. This is because thermal noise will lead to transient flucutations in the periphery of the steric layers, leading at times to attractive excluded volume interactions between two steric layers. The particles will be sterically stabilized only when $N > N_{cross}$.

As the solvent becomes poorer ($\nu \ll f^{1/2}$), the density in the dense inner layer becomes *nearly* constant, with a value $\Phi \approx -3/2\nu$ after an initial drop from unity near the center of the star. One must bear in mind, however, the caveat that while the truncated virial equation is useful for obtaining some analytical solutions for the equations in section 2, they do not bring out the density saturation effects that must be important in very poor solvents where the density tends to unity. We believe that analytical solutions using the virial equation of state would be of limited validity in very poor solvents.

5. Collapse Induced by *n*-Clusters

Recently, de Gennes has advanced the notion of n-clusters for water-soluble polymers (which are not polyelectrolytes) where some higher order ($n > 2$) segment

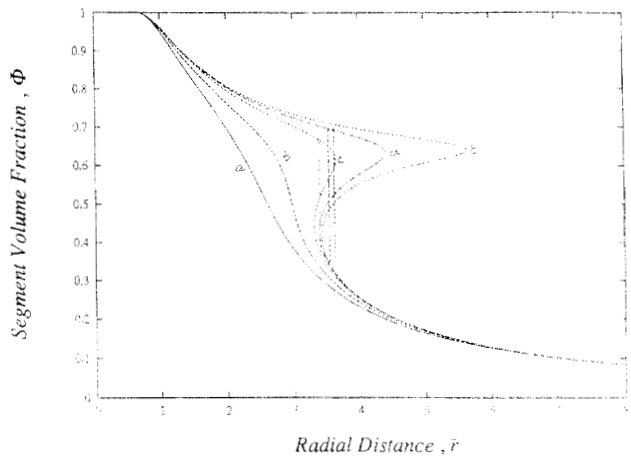

Figure 7. Reduced segment density profiles for stars and spherical brushes using the n-cluster theory. Equation 23 was used for calculating the osmotic pressure ($n = 3$, $\rho^* = 0.67$). The n-cluster parameters ρ are (a) 0.6, (b) 0.67, (c) 0.7, (d) 0.72, and (e) 0.727. The vertical lines show the discontinuous drop in the density.

interactions can become attractive even while binary ($n = 2$) interactions are repulsive. It is obvious that a hierarchy of forces similar to polyelectrolytes in poor solvents exists here also. In the polyelectrolyte case the longer range force (electrostatics, $\Pi \sim \Phi$) was repulsive while the shorter range force (binary, $\Pi \sim \Phi^2$) was attractive. This leads to a two-phase brush with an inner dense layer and an outer dilute layer. For n-cluster-induced collapse we have a longer range repulsive force (binary, $\Pi \sim \Phi^2$) and a shorter range attractive force (n-cluster, $\Pi \sim \Phi^n, n > 2$). Indeed Wagner et al.[32] have already shown, using the MWC SCF[4] theory, that for planar brushes collapsed by n-clusters one obtains an inner dense layer (n-clusters dominate) and an outer dilute layer (binary repulsions stretch the chains). They used the following EOS for the polymer solution

$$F(\Phi) = (1 - \Phi)\ln(1 - \Phi) + \rho(\Phi - \Phi^n) \qquad (23)$$

which reduces to the Flory–Huggins theory if $n = 2$ and if one replaces ρ with χ. For $n > 2$ this implies that binary interactions are athermal (repulsive) while the higher order interactions can become attractive. The switch from a good to a bad solvent occurs when $\rho \geq \rho^*$, where

$$\rho^* = \frac{1}{n}\left(\frac{n-1}{n-2}\right)^{n-2} \qquad (24)$$

The osmotic pressure is given as

$$\Pi_{n\text{-cluster}} = -\ln(1 - \Phi) - (n - 1)\rho\Phi^n - \Phi \qquad (25)$$

Substituting this expression for the osmotic pressure in the equations in the previous section, one obtains a collapse behavior that is qualitatively similar to the collapse of the polyelectrolyte brush in a poor solvent. There appears to be some experimental evidence for the n-cluster-induced collapse of adsorbed layers of poly(N-isopropylacrylamide) in the work of Zhu and Napper.[45] The collapse in these experiments, observed to be continuous and over a broad range of temperatures, is rationalized by Zhu and Napper as occurring by attractive n-cluster interactions. The predictions of the model presented in this work also point toward a continuous collapse (rather than first order) induced by n-clusters. Typical segment density profiles and the Maxwell constructions are shown in Figure 7.

6. Conclusions

In this work we present a simple model for spherical brushes and stars where all chain ends lie at the same outer shell and the local structure is determined by a local balance between the stretching of chains and the local osmotic pressure. We look at the general features of polyelectrolyte stars (and brushes) in good and poor solvents and find that there are four distinct regions where the density profile is dominated by one or the other of the interactions: (i) in the outer regions ($r > r_3 \sim (\sigma\nu/f)^{1/2}$) the density is dominated by electrostatics and $\Phi \sim r^{-2}$, (ii) in the intermediate region ($r_2 \sim \sigma^{1/2}\nu^{-1} < r < r_3$) binary interactions dominate and $\Phi \sim r^{-4/3}$, (iii) in the inner region ($r_1 \sim \sigma^{1/2} < r < r_2$) ternary interactions dominate and the density profile $\Phi \sim r^{-1}$, and finally (iv) at the center of the star the density is unity. In poor solvents the density profile shows a discontinuous change from an inner dense layer (dominated by ternary repulsions) to an outer dilute layer (dominated by electrostatic repulsions)—the intermediate density region that exists for good solvents is eliminated. In good solvents ($\nu > 0$) the crossover from a polyelectrolyte-dominated regime to a binary repulsion regime is determined by $N_{P\to B} \sim (\sigma\nu)^{1/2}f^{-5/4}$. In poor solvents the crossover is between electrostatic and ternary regimes and is determined by $N_{P\to T} \sim \sigma^{1/2}|\nu|f^{-3/2}$. The location of the discontinuity between the inner and outer regions is determined by a Maxwell construction. A similar qualitative picture also emerges for uncharged water-soluble polymer stars or spherical brushes that are collapsed by n-clusters. Finally, the magnitude of collapse for spherical polyelectrolyte brushes and stars strongly depends upon the chain length (unlike for planar brushes) and hence is much more pronounced for these convex geometries. The collapse transition itself appears to be continuous since the change in segment density distributions with solvent quality or backbone charge is continuous and thus implies a smooth change from swollen to collapsed stars or brushes (although it may appear "first-order-like" because of the magnitude of change over a short range of parameters). The validity of the predictions detailed in this paper can be tested experimentally by using SANS techniques to determine the segment density distribution functions in appropriate systems.[46] The nature of the transition itself could be determined by probing the changes in the hydrodynamic size (using dynamic light scattering) of a colloidal particle with long end-grafted chains.

Acknowledgment. D.H.N. thanks the Australian Research Council for support of these studies.

Appendix 1: Cylindrical Brushes

We present here the corresponding results for cylindrical polyelectrolyte brushes which would also have relevance to graft copolymers where we have long side chains grafted onto a backbone chain (cylinder of radius zero). Assuming that σ chains are grafted per unit length of the copolymer (or alternately that σ_0 chains are grafted per unit area of a cylinder of radius r_0), we can write the following force balance equation

$$\Phi\Pi = \frac{\sigma^2}{4\pi r^2} = \frac{\sigma_0^2 r_0^2}{r^2} = \frac{1}{\tilde{r}^2} \qquad (A.1.1)$$

Good Solvent Regime ($\nu > 0$). Using the virial equation of state (eqs 6a,b), we obtain, analogous to star polyelectrolytes, that there are four distinct segment density regions. In the outermost region, r_3 ($\sim \sigma\nu f^{3/2}$) $< r$ we have

electrostatic domination

$$\Phi \sim \sigma f^{-1/2} r^{-1}, \quad \text{outermost region } (r_3 < r) \quad \text{(A.1.2)}$$

This implies that the stretch rate is a constant in the electrostatic region, as with stars and spherical brushes. In the intermediate region, r_2 ($\sim \sigma\nu^{-2}$) $< r < r_3$, binary interactions dominate and the density profile obeys

$$\Phi \sim \sigma^{2/3}\nu^{-1/3} r^{-2/3}, \quad \text{intermediate region } (r_2 < r < r_3) \quad \text{(A.1.3)}$$

In the inner region, r_1 ($\sim \sigma\nu^{-2}$) $< r < r_2$, ternary interactions dominate and the density profile obeys

$$\Phi \sim \sigma^{1/2} r^{-1/2}, \quad \text{inner region } (r_1 < r < r_2) \quad \text{(A.1.4)}$$

Finally for $r < r_1$, $\Phi \approx 1$ (meltlike region).

The dimensions of the cylindrical brush or side chains in the graft copolymer (bottle brush) in different regimes are

$$R_P \sim \sigma^0 f^{1/2} N^1, \quad \text{polyelectrolyte dominated } (\sigma\nu f^{-2} \ll N) \quad \text{(A.1.5a)}$$

$$R_B \sim \sigma^{1/4}\nu^{1/4} N^{3/4}, \quad \text{binary interactions dominated } (\sigma\nu^{-3} \ll N \ll \sigma\nu f^{-2}) \quad \text{(A.1.5b)}$$

The crossover from the electrostatic regime to the binary regime occurs at $N_{P\to B} \sim \sigma\nu f^{-3/2}$. For ternary-dominated bottle brushes we have

$$R_T \sim \sigma^{1/3} N^{2/3}, \quad \text{ternary repulsions dominated } (\sigma \ll N \ll \sigma\nu^{-3}) \quad \text{(A.1.5c)}$$

and

$$R_D \sim \sigma^{1/2} N^{1/2}, \quad \text{completely collapsed} \quad \text{(A.1.5d)}$$

Note that in the ratios R_P/R_B ($\sim N^{-1/4}$) and R_B/R_D ($\sim N^{-1/4}$) the dependence on N, for cylindrical polyelectrolyte brushes, is weaker than that for spherical brushes (eqs 15 and 16). For planar brushes the N dependence of the corresponding ratios vanishes completely.[22] The magnitude of the collapse in cylindrical brushes is stronger than that for planar brushes but smaller than that for spherical brushes. The N dependence is greatest for geometries where the packing constraints are the weakest.

Poor Solvent ($\nu < 0$). The density profiles again go from being single valued to two valued at the critical conditions described by eq 19. The Maxwell construction is exactly along the lines described for stars and spherical brushes except that the EOS is the one implied by eq A.1.1.

We estimate that the value of the minimum distance for a discontinuous density drop, ρ_1, obeys the following equation:

$$\rho_1 \sim \sigma|\nu| f^{-3/2} \quad \text{(A.1.6)}$$

Assuming again that ternary interactions dominate the inner dense layer, we can again calculate a crossover chain length, N_{cross}, that separates a "single-phase" totally collapsed brush from a "two-phase" brush.

$$N_{cross} \sim \sigma|\nu|^{3/2} f^{-1} \quad \text{(A.1.7)}$$

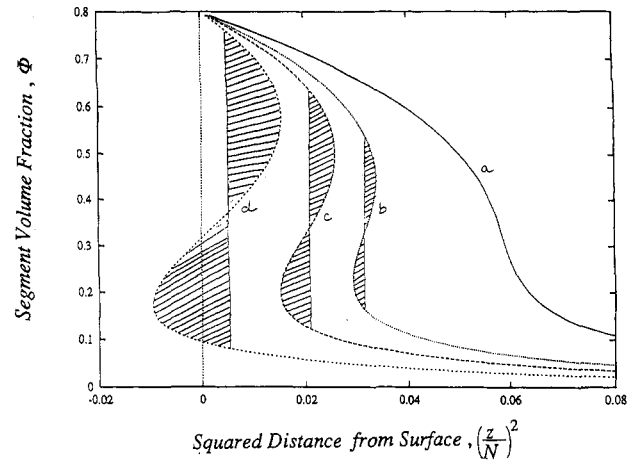

Figure 8. Typical segment density profiles for a planar brush for a given surface volume fraction of 0.8. The charge fraction is 0.1. Equation 6b was used for calculating the osmotic pressure. The excluded volume parameters, ν, are (a) −0.6, (b) −0.67, (c) −0.7, and (d) −0.75.

Appendix 2: Planar Brushes

In this section we show that even a planar polyelectrolyte brush can collapse into a two-phase brush by going into the poor solvent regime. For this one needs to use the SCF theory of MWC since the Alexander–de Gennes type model produces a uniform density inside the planar brush. Indeed the case of planar brush collapse induced by n-clusters has been analyzed by Wagner et al. in this SCF picture.[32] We employ the same methodology as Wagner et al. to deduce the density profile for collapsed planar polyelectrolyte brushes.

The chemical potential of the segments varies as follows:[4]

$$-U = \frac{\partial F}{\partial \Phi} = A - Bz^2 \quad \text{(A.2.1)}$$

where A is a constant (wall potential) for a given grafting density, $B = (\pi^2/8N^2)$, and z is the distance from the grafting surface. Substituting the virial expansion for F, we obtain

$$A - Bz^2 = \nu\Phi + \frac{1}{2}\Phi^2 + f \ln \Phi \quad \text{(A.2.2)}$$

We determine some typical segment density profiles for given values of A and f and different values of the excluded volume parameter ν. (This corresponds to different grafting densities. One can, however, do the reverse process of determining the grafting density given a value of A, which is easier.) Note that the osmotic pressure goes to zero when $z \to \infty$; in other words, the brush is infinitely long! However, the density drops to a very low value well before $z = N$, and therefore this is not a major concern. (Solving the full Poisson–Boltzmann equation instead of assuming local electroneutrality will alleviate this problem since the nonzero electric field will contribute to the pressure; this will lead to a zero osmotic pressure at a finite distance $z = h$; $\Phi(h) \neq 0$ in general.) But for the present purpose eq A.2.2 will be sufficient.

The Maxwell construction, as outlined by Wagner et al., is straightforward for planar brushes since the right-hand side of eq A.2.2 is nothing but the chemical potential

of the segments. Since U and Φ are conjugate variables (like p and V), a plot of U vs Φ provides the equal-area construction needed to locate the discontinuity. Since $U \sim z^2$, one needs to plot Φ vs z^2 to do the equal-area construction. Some typical segment density profiles are shown in Figure 8.

References and Notes

(1) Halperin, A.; Tirrell, M.; Lodge, T. P. *Adv. Polym. Sci.* **1992**, *100*, 31.
(2) Alexander, S. *J. Phys.* (*Paris*) **1977**, *38*, 983.
(3) de Gennes, P.-G. *Adv. Colloid Interface Sci.* **1987**, *27*, 189.
(4) Milner, S. T.; Witten, T. A.; Cates, M. E. *Macromolecules* **1988**, *21*, 2610.
(5) Skvortsov, A. M.; Gorbunov, A. A.; Pavlushkov, I. E.; Zhulina, E. B.; Borisov, O. V.; Priamitsyn, V. A. *Polym. Sci. USSR* (*Engl. Transl.*) **1988**, *30*, 1706.
(6) Halperin, A. *J. Phys. Fr.* **1988**, *49*, 547.
(7) Halperin, A.; Zhulina, E. B. *Macromolecules* **1991**, *24*, 5393.
(8) Zhulina, E. B.; Borisov, O. V.; Pryamitsyn, V. A.; Birshtein, T. M. *Macromolecules* **1991**, *24*, 140.
(9) Lai, P. Y.; Halperin, A. *Macromolecules* **1992**, *25*, 6693.
(10) Lai, P. Y. *Comput. Polym. Sci.* **1992**, *2*, 157.
(11) Shim, D. F. K.; Cates, M. E. *J. Phys. Fr.* **1989**, *50*, 3535.
(12) Halperin, A.; Zhulina, E. B. *Europhys. Lett.* **1991**, *16*, 337.
(13) Johner, A.; Joanny, J. F. *Europhys. Lett.* **1991**, *15*, 265.
(14) Zhulina, E. B.; Pakula, T. *Macromolecules* **1992**, *25*, 754.
(15) Milner, S. T.; Witten, T. A. *Macromolecules* **1992**, *25*, 5495.
(16) Halperin, A.; Zhulina, E. B. *Macromolecules* **1992**, *25*, 5730.
(17) Misra, S.; Mattice, W. L. *Macromolecules* **1994**, *27*, 2058.
(18) Pincus, P. *Macromolecules* **1991**, *24*, 2912.
(19) Borisov, O. V.; Birshtein, T. M.; Zhulina, E. B. *J. Phys. II* **1991**, *1*, 521.
(20) Zhulina, E. B. *Macromolecules* **1993**, *26*, 6273.
(21) Ross, R.; Pincus, P. *Macromolecules* **1992**, *25*, 2177.
(22) Argillier, J. F.; Tirrell, M. *Theor. Chim. Acta* **1992**, *82*, 343.
(23) Wittmer, J.; Joanny, J. F. *Macromolecules* **1993**, *26*, 2691.
(24) Dan, N.; Tirrell, M. *Macromolecules* **1993**, *26*, 4310.
(25) Miklavic, S. J.; Marcelja, S. *J. Phys. Chem.* **1988**, *92*, 6718.
(26) Misra, S.; Varanasi, S.; Varanasi, P. P. *Macromolecules* **1989**, *22*, 4173.
(27) Misra, S.; Varanasi, S. *Macromolecules* **1991**, *24*, 322.
(28) Misra, S.; Varanasi, S. *J. Chem. Phys.* **1991**, *95*, 2183.
(29) Zhulina, E. B.; Borisov, O. V.; Birshtein, T. M. *J. Phys. II* **1992**, *2*, 63.
(30) Misra, S.; Varanasi, S. *Macromolecules* **1993**, *26*, 4184.
(31) de Gennes, P.-G. *C. R. Acad. Sci. Paris II* **1991**, *313*, 1117.
(32) Wagner, M.; Brochard-Wyart, F.; Hervet, H.; de Gennes, P.-G. *Colloid Polym. Sci.* **1993**, *271*, 621.
(33) Daoud, M.; Cotton, J. P. *J. Phys. Fr.* **1982**, *43*, 531.
(34) Birshtein, T. M.; Zhulina, E. B. *Polymer* **1984**, *25*, 1453.
(35) Witten, T. A.; Pincus, P.; Cates, M. E. *Europhys. Lett.* **1986**, *2*, 137.
(36) Halperin, A.; Alexander, S. *Macromolecules* **1987**, *20*, 1146.
(37) Ball, R. C.; McLeish, T. C. B. *Macromolecules* **1989**, *22*, 1911.
(38) Raphael, E.; Pincus, P.; Fredrickson, G. H. *Macromolecules* **1993**, *26*, 1996.
(39) Miyake, A.; Freed, K. F. *Macromolecules* **1983**, *16*, 1228.
(40) Freire, J. J.; Rey, A.; Garcia de la Torre, J. *Macromolecules* **1986**, *19*, 457.
(41) Lipson, J. E. G.; Gaunt, D. S.; Wilkinson, M. K.; Whittington, S. G. *Macromolecules* **1987**, *20*, 186.
(42) Grest, G. S.; Kremer, K.; Milner, S. T.; Witten, T. A. *Macromolecules* **1989**, *22*, 1904.
(43) Grest, G. S.; Kremer, K.; Witten, T. A. *Macromolecules* **1987**, *20*, 1376.
(44) Ball, R. C.; Marko, J. F.; Milner, S. T.; Witten, T. A. *Macromolecules* **1991**, *24*, 693.
(45) Zhu, P. W.; Napper, D. H. *J. Colloid Interface Sci.* **1994**, *164*, 489.
(46) Fleer, G. J.; Cohen-Stuart, M. A.; Scheutjens, J. M. H. M.; Cosgrove, T.; Vincent, B. *Polymers at Interfaces*; Chapman and Hall: London, 1993; pp 369–370.